

## Development and Validation of a Liquid Chromatography–Electrospray Ionization–Time-of-Flight Mass Spectrometry Method for Induced Changes in *Nicotiana attenuata* Leaves during Simulated Herbivory

EMMANUEL GAQUEREL,<sup>\*,†</sup> SVEN HEILING,<sup>†</sup> MATTHIAS SCHOETTNER,<sup>†</sup>  
GABRIELA ZUREK,<sup>‡</sup> AND IAN T. BALDWIN<sup>†</sup>

<sup>†</sup>Department of Molecular Ecology, Max Planck Institute for Chemical Ecology, Hans-Knöll-Strasse 8, 07745 Jena, Germany, and <sup>‡</sup>Bruker Daltonik GmbH, Bremen, Germany

A liquid chromatography–electrospray ionization–time-of-flight mass spectrometry (HPLC/ESI-TOF-MS) procedure was developed to characterize changes induced in *Nicotiana attenuata* leaves 1 h and 5 days after wounding and application of *Manduca sexta* elicitors. The constancy of the measurement conditions was first confirmed for 22 selected analytes spanning the entire chromatogram. Using the Profile Analysis software, we extracted 367 buckets, which were analyzed by principal component analysis and two-factorial ANOVA. One hundred seventy-three buckets were found to be statistically regulated, 128 due to time effects, and 85 due to treatment effects. In vivo <sup>15</sup>N-isotope labeling was used to facilitate the annotation and the interpretation of the fragmentation pattern of nitrogen-containing metabolites, and a correlation analysis was performed to test mathematical relationships existing among potential in-source fragments. Additionally, tandem MS measurements of the most regulated ions are presented. Altogether, this study defines a framework for the mining and annotation of major herbivory-elicited changes in *Nicotiana attenuata*.

**KEYWORDS:** *Nicotiana attenuata*; metabolomics; HPLC-ESI/TOF-MS; phenylpropanoid–polyamine conjugates; diterpene glycosides

### INTRODUCTION

Plants use a variety of induced responses to protect themselves from insects (1). The fine-tuned regulation of these responses allows plants to decrease the costs of constitutive defense production but also optimize their ability to compete with neighboring plants or to tolerate the damage from specialized herbivores. Such adaptative changes require significant reorganization of metabolic pathways. Hence, obtaining the broadest, unbiased analysis of a plant's metabolism is essential for an understanding of the molecular bases of the plasticity that plants exhibit in the face of ecological challenges. The wild tobacco *Nicotiana attenuata* is equipped with a suite of inducible metabolites whose functions and regulations have been extensively studied in the laboratory and field conditions. Nicotine, a neurotoxin which functions synergistically with antidigestive plant proteins (2) and members of the diterpene glycoside family (3), collectively compromises insect performance and is the most active and best characterized of the defense compounds produced by a plant. Diterpene glycosides and sucrose esters are among the most abundant leaf metabolites in *N. attenuata* (Figure 1). Additionally, phenylpropanoid–polyamine conjugates also increase in concentration in insect-damaged plants, and some of these have been shown to improve the plant's resistance to insects when sprayed onto attacked leaves (4).

Research into the response of plants to herbivore attack has been traditionally dominated by the analysis of single metabolic pathways that are thought by the researcher to be important for defenses. The dramatic developments and decreasing costs of omic tools allow researchers to ask the plant how it regulates genes, proteins, and classes of metabolites in response to different biotic and abiotic stresses. Such omic analyses applied to the interaction between *N. attenuata* and the lepidopteran larva *M. sexta* have demonstrated that more than ~300 transcripts (5), 90 proteins (6), and the emission of 35 volatile organic compounds (7) are significantly regulated by attack from *M. sexta* larvae.

Metabolomics, which is defined as the comprehensive, quantitative, and qualitative measurement of the metabolite signature within a cell, tissue, or organism, has been suggested to be the ultimate level of omic analyses as it reflects both transcriptional and post-transcriptional regulation. Temperature and nutritional stresses have been the most comprehensively characterized by nontargeted metabolite profiling. Several studies have investigated wound-induced changes in the leaf metabolome (8–10); but few biotic interactions have been explored from a metabolomic standpoint. Allwood et al. (11) could distinguish the metabolic fingerprints of susceptible and resistant *Brachypodium distachyon* plants challenged by the fungal pathogen *Magnaporthe grisea*. The MS-based metabolic analyses performed by Jansen et al. (12) monitored the chemical changes in cabbage plant leaves and in the digestive tract of feeding *Pieris rapae* larvae to understand

\*Corresponding author. Tel: 49-(0)3641-571100. Fax: 49-(0)3641-571102. E-mail: egaquerel@ice.mpg.de.

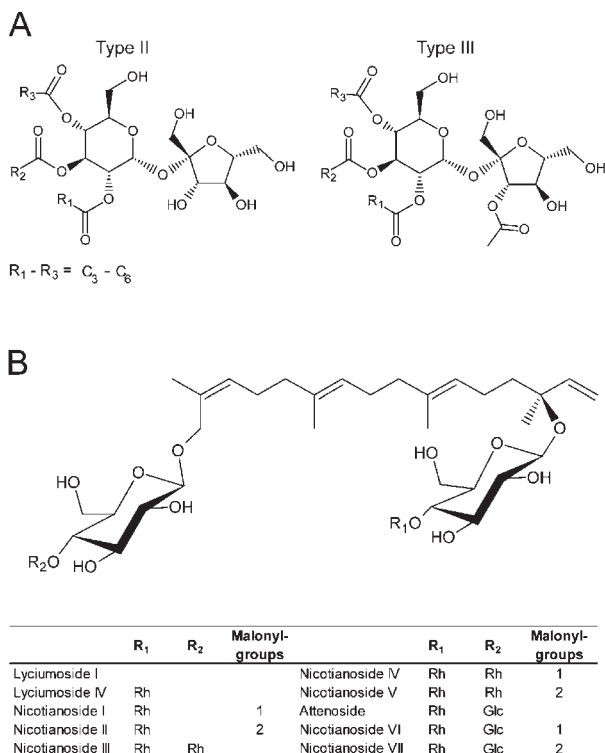


**Figure 1.** *Nicotiana attenuata* sucrose esters and 17-hydroxygeranylinalool diterpene glycosides. (A) Sucrose esters are esterified by short chain fatty acids ranging from three to six carbons in chain length. Type III sucrose esters are acetylated at their fructose moiety (28). (B) Diterpene glycosides differ in their sugar (Rh, rhamnose; Glc, glucose) and malonyl groups (23).

the metabolite exchanges at the plant–insect interface. Kuzina et al. (13) identified two main clusters of metabolites that correlated negatively with flea beetle survival in an F2 population of susceptible and resistant Winter cress parents.

Although the chemical diversity of the plant metabolome cannot be comprehensively resolved using a single procedure, different analytical techniques have been optimized to produce metabolic profiles. Among these, the combination of the high analytical precision of modern high/ultrahigh pressure liquid chromatography techniques (HPLC/UPLC) with the mass accuracy and resolution of modern mass spectrometry (MS) has emerged as a method of choice for profiling leaf extracts; although, contrary to gas chromatography-MS, no exhaustive databases exist. Current orthogonal acceleration time-of-flight (TOF) MS analyzers are routinely used for the determination of elemental formulas which can notably be assisted by the use of *in vivo* isotope labeling of the entire metabolome using  $^{13}\text{C}_2$ . However, the complexity inherent to the interpretation of mass spectra stems from the fact that all metabolites can fragment by the loss of neutral moieties. Targeted collision-induced dissociation (CID)-MS/MS experiments performed for relevant pseudo-molecular ions or in-source fragments add information important for the description of this fragmentation process. Importantly, nontargeted analysis requires that mass signals are extracted from raw data files and their retention time corrected. This task can be performed by using commercially available software such as Markerlynx or Profile Analysis or freeware such as XCMS (14). However, none of these procedures can comprehensively recognize and assemble in-source fragments. Correlation analysis of ESI-MS data features can potentially be performed to confirm relationships of in-source fragments.

In this study, we investigated the application of a rapid and generic HPLC-ESI/TOF-MS procedure to explore changes in *N. attenuata* leaf chemistry induced during simulated herbivory. HPLC-MS data was prepared for statistical analysis using two different peak detection and bucketing procedures and analyzed by principal component analysis as well as by two-factorial ANOVA to both highlight candidate buckets responsible for group separation and calculate the degree of significance associated with their changes in intensity. *In vivo*  $\text{K}^{15}\text{NO}_3$ -based isotope labeling, correlation analysis of in-source fragments, and tandem MS experiments performed for the annotation of the most promising ions are presented.

## MATERIALS AND METHODS

**Plant Material.** We used an isogenic line, obtained after 30 generations of inbreeding, of *Nicotiana attenuata* from field-collected seeds. Seeds were germinated as described in Krügel et al. (15). All plants were grown in the glasshouse in 1 L individual pots at 26–28 °C under 16 h of light supplied by Philips Sun-T Agro 400- or 600-W sodium lights (Philips, Turnhout, Belgium). For *in vivo*  $^{15}\text{N}$ -labeling, plants were grown in hydroponic solutions containing  $\text{K}^{15}\text{NO}_3$  (98%  $\text{K}^{15}\text{NO}_3$ , Sigma-Aldrich, Steinheim, Germany) as the sole nitrogen source.

Metabolic changes induced during *Manduca sexta* feeding were reproduced by producing with a fabric pattern wheel three rows of puncture onto each side of the midvein of five fully expanded leaves per plant (5 biological replicates) and directly applying 1:1 diluted *M. sexta* oral secretions (OS). Treated leaves from the same plant were harvested, pooled, and flash frozen 1 h and 5 days after elicitation. Control leaves were left unwounded and harvested from other plants at the same time points. Leaves from plants grown on  $\text{K}^{15}\text{NO}_3$ -containing hydroponic solutions were treated as described above but harvested 3 days after treatment.

**Sample Preparation.** One hundred milligrams of ground leaf tissue was weighted and transferred to a Fast Prep tube containing 0.9 g of Fast Prep matrix (BIO 101, Vista, USA). One milliliter of extraction buffer per 100 mg of tissue [50 mM acetate buffer, pH 4.8, containing 40% methanol spiked with reserpine (600 ng/mL), atropine (200 ng/mL)] was added, and the samples were homogenized. After centrifugation (13.2 rpm, 20 min, 4 °C), the supernatant was collected in a fresh 1.5 mL Eppendorf tube and centrifuged again, and 100  $\mu\text{L}$  of the supernatant was transferred to a HPLC vial.

**HPLC/ESI-TOF-MS.** Two microliters of the leaf extract were separated using a HPLC 1100 Series system (Agilent, Palo Alto, USA). The column used was a 150 mm  $\times$  2 mm i.d., 3  $\mu\text{m}$ , Phenomenex Gemini NX RP-18 column with a 2 mm  $\times$  4 mm i.d. guard column of the same material (Phenomenex, Germany). The following binary gradient was applied: 0 to 2 min isocratic 95% A (deionized water, 0.1% [v/v] acetonitrile [Baker, HPLC grade], and 0.05% formic acid), 5% B (acetonitrile and 0.05% formic acid); 2 to 30 min linear gradient to 80% B; isocratic for 5 min. The flow rate was 200  $\mu\text{L}/\text{min}$ .

Eluted compounds were detected by a MicroToF mass spectrometer (Bruker Daltonik, Bremen, Germany) equipped with an electrospray ionization source in positive and negative ion modes. Typical instrument settings were as follows: capillary voltage, 4500 V; capillary exit, 130 V; dry gas temperature, 200 °C; dry gas flow, 8 L/min. Ions were detected from  $m/z$  200 to 1400 at a repetition rate of 1 Hz. Mass calibration was performed using sodium formate clusters (10 mM solution of NaOH in 50/50% v/v isopropanol/water containing 0.2% formic acid).

**HPLC/ESI-qTOF-MS.** Selected samples were subjected to targeted HPLC-MS/MS experiments using the chromatographic conditions described above but using a Dionex RSLC system (Dionex, Sunnyvale, USA). MS detection was carried out with a maXis ESI-qTOF mass spectrometer (Bruker Daltonik, Bremen, Germany) operated in electrospray positive mode. Typical instrument settings were as follows: capillary voltage, 4500 V; dry gas temperature, 200 °C; dry gas flow, 8 L/min; capillary exit, 117 V; funnel, RF 300 Vpp. Ions were detected from  $m/z$  50 to 1300 at a repetition rate of 1 Hz. The instrument was operated in autoMS/MS mode using a scheduled precursor list (SPL) of ions selected for MS/MS experiments. The SPL was generated on the basis of the

statistical results. Mass calibration was performed using sodium formate clusters (10 mM solution of NaOH in 50/50% v/v isopropanol/water containing 0.2% formic acid).

**Advanced Bucketing Using Profile Analysis.** Buckets are  $m/z$  and retention time windows of adjustable size, which summarize the intensity of all signals in the respective window. Data sets were evaluated from 60 to 1500 s in the mass range  $m/z$  90 to 1400 using Profile Analysis (Bruker Daltonik, Bremen, Germany). Compound finding was performed prior to advanced bucketing using the find molecular feature (FMF) algorithm (16). On the basis of the line mass spectra, mass peak clusters which consist of a minimum number of consecutive scans (minimum compound length = 8) are generated. No gaps larger than one spectrum are allowed within the cluster. Peaks are added to the best matching cluster within a mass distance derived from the mass peak width. Local extracted ion chromatograms (EIC) traces are calculated from the clusters. Chromatographic peak detection ( $S/N = 3$ , no smoothing) is performed on these EIC traces allowing the subsequent correlation analysis of neighboring isotopes (correlation coefficient threshold = 0.7, maximum value = 1.0). Charge states are created by a combination of peak clusters having a high correlation in retention time and the matching  $m/z$  value distances for  $z > 1$ . In a final step, compounds are assembled with related isotopes and charge states as well as chromatographic peak information. The advanced bucketing based on the compounds detected with the above-described algorithm was performed using the tolerance values  $\Delta Rt$  (66.03 s) and  $\Delta m/z$  (7.40 mDa) information obtained from the time alignment. During this process, all compounds of an HPLC-MS run are aligned to a master run in a pair wise comparison. Buckets with multiple compounds were divided. Buckets detected in 4 out of the 5 biological replicates of a group attribute were considered for statistical analysis. The bucket intensity values in one sample were normalized to the total intensity (sum of all bucket values) in the sample.

**XCMS Data Processing.** Raw data files were converted to the netCDF format using the export function of the Data Analysis v4.0 software (Bruker Daltonik, Bremen, Germany) and processed using the XCMS package (14). XCMS combined with statistical analysis was used as an independent peak picking procedure to support herbivory-regulated compounds detected using the Profile Analysis software. Peak detection was performed using the centWave method (14) and the parameter settings ppm = 20, snthresh = 10, peakwidth = 20 to 50 s. Retention time correction was achieved using the parameter settings minfrac = 1, bw = 60 s, mzwid = 0.1 D, span = 1, and missing = extra = 0. After peak grouping and filling in of missing features using the fillPeaks routine of the XCMS package, the obtained data matrix was imported into Microsoft Excel for statistical analysis. Consistent mass features, which were at least present (for a single sampling time and treatment) in four out of the five biological replicates with an  $Rt > 1$  min, an  $m/z > 120$  and an average intensity  $> 10,000$ , after normalization to the sum of the integration values of all consistent mass features, were considered for further analysis.

**Elemental Formula Calculation and Structure Elucidation.** For molecular formula generation using the SmartFormula algorithm (DataAnalysis 4.0 software, Bruker Daltonik, Bremen), the following maximum elemental composition  $C_aH_bN_cO_dNa_eK_f$  and restrictions were used:  $1 \leq b/a \leq 3$ ;  $e = 0$  or  $1$ ;  $f = 0$  or  $1$ ;  $a, b, c,$  and  $d$  not limited. Rings plus double bonds values from  $-0.5$  to  $40$ , the nitrogen rule, and ions of even electron configuration were considered. Formulas were ranked according to both mass deviation and isotope pattern accuracy reflected in the sigma value. The sigma value is inversely proportional to the quality of the fit between the calculated isotope pattern of the predicted elemental formula and the measured isotope pattern of the ion considered during the analysis. For nitrogen-containing metabolites, the number of nitrogen atoms was deduced from the analysis of  $K^{15}NO_3$ -based isotope labeled *N. attenuata* leaf extracts. Correlation analysis of ESI-MS data features was used to confirm the predicted relationships and then group ionization products. Additionally, elemental formula calculation was improved by the analysis of MS/MS data, the SmartFormula 3D algorithm, and the elemental formula restrictions described above. The algorithm first suggests a list of formulas based on the MS spectrum and then automatically calculates the sum formulas of the CID-MS/MS fragments. As the fragment-ions must be a subset of the precursor-ion, usually just a few formulas remain.

MS and MS/MS data of leaf metabolites were compared with those of authentic standards when available. In addition, manual annotation using

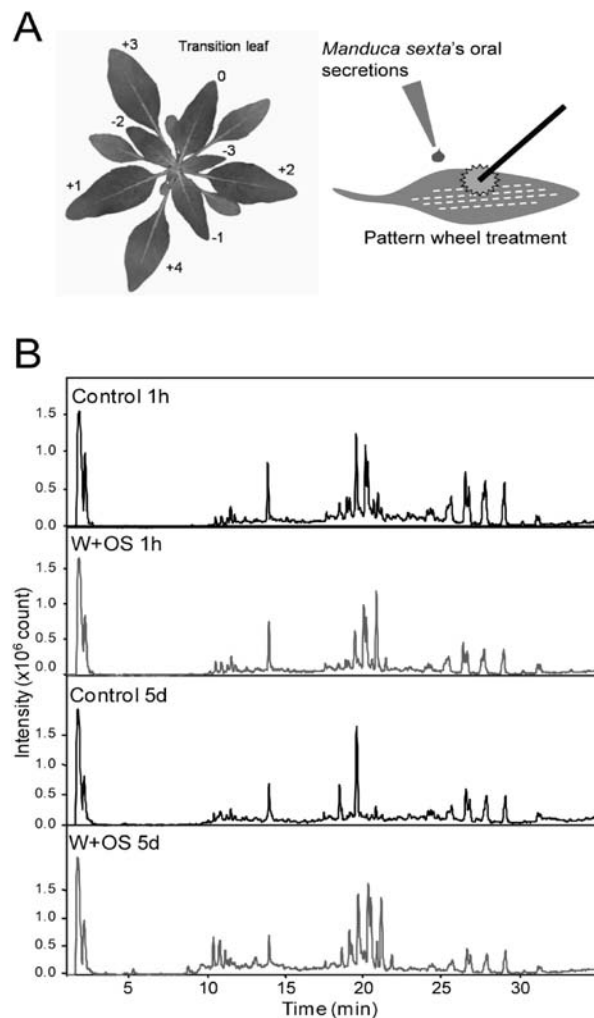


**Figure 2.** Experimental design, representative chromatograms, and processing work-flow. (A) Left: numbering system of leaf nodes of 30-day-old rosette-stage *Nicotiana attenuata* plants. Right: the leaf-wounding procedure with the pattern wheel and treatment with *Manduca sexta* oral secretions (W+OS). W+OS-treated and untreated leaves were harvested 1 h (control 1 h and W+OS 1 h) and 5 days (control 5 days and W+OS 5 days) after the start of the experiment. (B) Representative HPLC-ESI/TOF-MS chromatograms.

metabolite information from the literature was also performed. The four levels of metabolite annotation recommended by the Metabolomics Standard Initiative were employed (17).

**Statistical Analysis.** PCA analysis was performed using Profile Analysis after PARETO scaling (18). The two-factorial ANOVA was performed using the normalized bucket table from Profile Analysis and the TIGR MultiExperiment Viewer software. Significance levels for correlation values ( $r$ ) were determined following the number of metabolite pairs ( $n$ ) using the equation  $t = r \times (n - 2)^{0.5} / (1 - r^2)^{0.5}$ . Correlation values at a significance level of 0.05 were visualized using heat maps generated with the TIGR MultiExperiment Viewer software.

## RESULTS AND DISCUSSION

**Method Validation.** We first assessed the reliability and robustness of mass signal detection and the reproducibility of extraction and measurement conditions. To this end, injection replicates of a single pooled leaf extract ( $N = 16$ ) were analyzed. Twenty-two analytes spanning the entire chromatogram and occurring at different orders of intensity ( $2.6 \times 10^3$  to  $1.6 \times 10^6$  counts) as well as 2 authentic standards (atropine and reserpine) spiked in

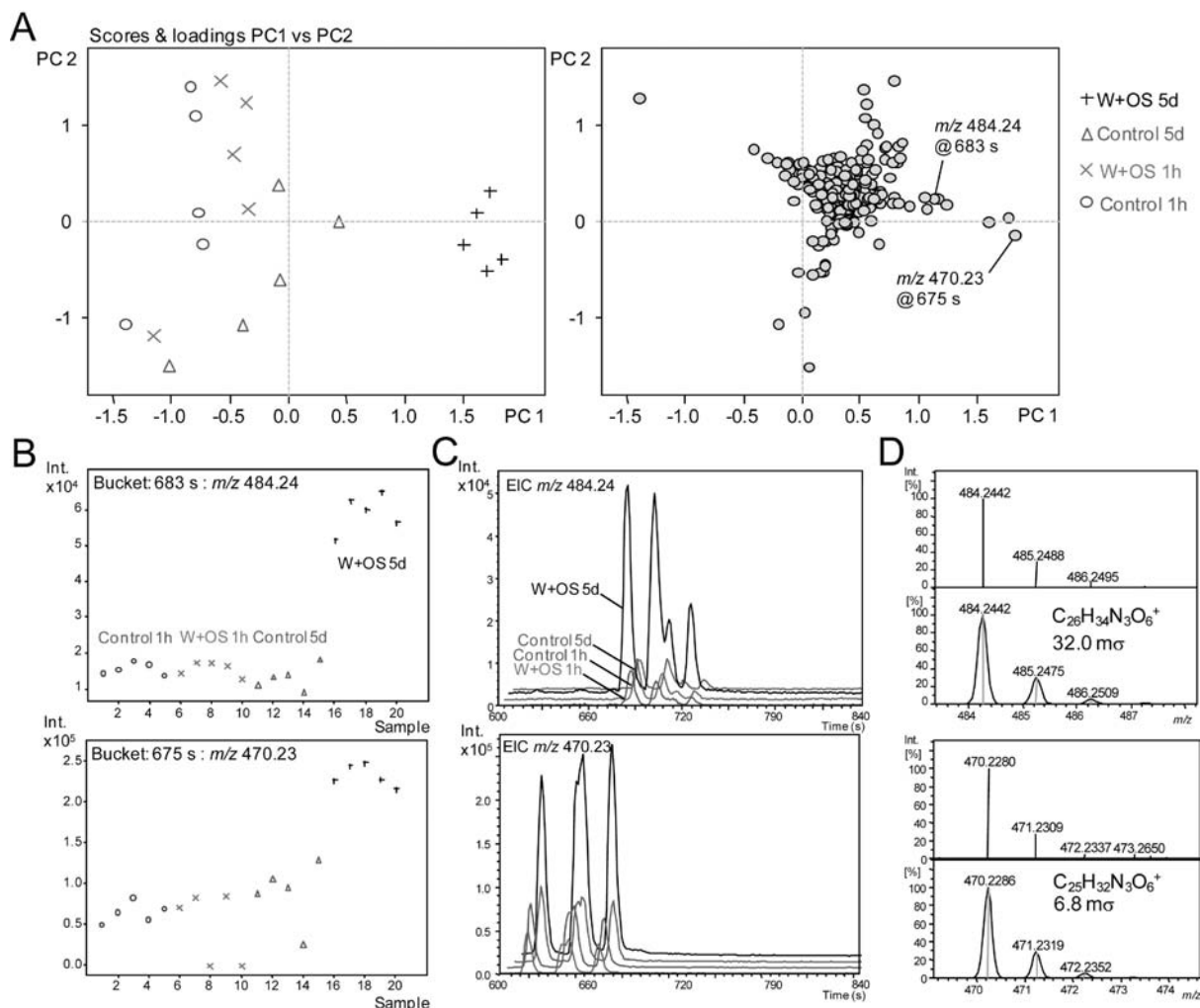


**Figure 3.** Principal component analysis and elemental formula calculation using Profile Analysis. **(A)** Projection plots obtained for principal component 1 (PC1, 51% variance explained) and PC2 (25%). Different motifs indicate different groups of treatments: control samples or induced by W+OS collected after 1 h (control 1 h and W+OS 1 h) or 5 days (control 5 days and W+OS 5 days). **(B)** Bucket statistics diagrams show differences across samples for one specific compound, here 484.24  $m/z$  at 684 s and 470.23  $m/z$  at 675 s. **(C)** Extracted ion chromatograms (EICs). **(D)** Comparison of measured and calculated isotopic distribution and predicted elemental formulas.

**Table 1.** Candidate Compounds and Proposed Molecular Formulas Derived from the PCA Model<sup>a</sup>

ID	bucket	El. F.	SigmaFit ( $m\sigma$ )	error (mDa)	annotation	
1	$m/z$ 470.23	at 675 s	$C_{25}H_{32}N_3O_6^+$	6.8	0.4	<sup>3</sup> <i>N,N'</i> -dicafeoyl-spermidine, [M + H] <sup>+</sup> , isomer#3
2	$m/z$ 470.23	at 656 s	$C_{25}H_{32}N_3O_6^+$	29.8	2.2	<sup>3</sup> <i>N,N'</i> -dicafeoyl-spermidine, [M + H] <sup>+</sup> , isomer#2
3	$m/z$ 470.23	at 631 s	$C_{25}H_{32}N_3O_6^+$	19.1	0.4	<sup>3</sup> <i>N,N'</i> -dicafeoyl-spermidine, [M + H] <sup>+</sup> , isomer#1
4	$m/z$ 502.25	at 528 s	$C_{33}H_{32}N_3O_2^+$	29.6	1.6	<sup>3</sup> <i>N,N'</i> -dihydrated-diferuloyl-spermidine, [M + H] <sup>+</sup>
5	$m/z$ 347.19	at 685 s	$C_{19}H_{27}N_2O_4^+$	6.9	2.4	<sup>4</sup> unidentified putrescine conjugate, [M + H] <sup>+</sup>
6	$m/z$ 484.24	at 684 s	$C_{26}H_{34}N_3O_6^+$	32.0	2.5	<sup>3</sup> <i>N'</i> -cafeoyl- <i>N'</i> -feruloyl-spermidine, [M + H] <sup>+</sup>
7	$m/z$ 568.3	at 787 s	$C_{31}H_{42}N_3O_7^+$	15.5	2	<sup>4</sup> unidentified spermidine conjugate, [M + H] <sup>+</sup>
8	$m/z$ 251.14	at 194 s	$C_{13}H_{19}N_2O_3^+$	8.6	0.7	<sup>3</sup> <i>N</i> -cafeoyl-putrescine, [M + H] <sup>+</sup>
9	$m/z$ 1031.46	at 1207 s	$C_{47}H_{76}O_{23}Na^+$	26.2	4.8	<sup>3</sup> nicotinoside IV, [M + Na] <sup>+</sup>
10	$m/z$ 498.26	at 747 s	$C_{27}H_{36}N_3O_6^+$	29.3	1.7	<sup>3</sup> <i>N,N'</i> -diferuloyl-spermidine, [M + H] <sup>+</sup> , isomer#1
11	$m/z$ 530.28	at 599 s	$C_{27}H_{36}N_3O_8^+$	32.7	2.3	<sup>3</sup> unidentified spermidine conjugate, [M + H] <sup>+</sup>
12	$m/z$ 498.26	at 727 s	$C_{27}H_{36}N_3O_6^+$	31.0	1.2	<sup>3</sup> <i>N,N'</i> -diferuloyl-spermidine, [M + H] <sup>+</sup> , isomer#2
13	$m/z$ 271.24	at 1221 s	$C_{20}H_{31}^+$	13.3	0.2	<sup>3</sup> nicotinoside VII, [M + H] <sup>+</sup> , fragment
14	$m/z$ 665.35	at 1289 s	$C_{35}H_{53}O_{12}^+$	12.0	3.2	<sup>1</sup> nicotinoside II, [M + H] <sup>+</sup> , fragment
15	$m/z$ 931.41	at 1289 s	$C_{44}H_{67}O_2^+$	18.6	4.9	<sup>1</sup> nicotinoside II, [M + H] <sup>+</sup>
16	$m/z$ 163.12	at 124 s	$C_{10}H_{15}N_2^+$	1.4	0.5	<sup>1</sup> nicotine, [M + H] <sup>+</sup>
17	$m/z$ 885.40	at 1219 s	$C_{41}H_{66}O_{19}Na^+$	16.1	3.7	<sup>1</sup> nicotinoside I, [M + Na] <sup>+</sup>
18	$m/z$ 845.41	at 1225 s	$C_{41}H_{65}O_{18}^+$	25.7	0.7	<sup>1</sup> nicotinoside I, [M + H] <sup>+</sup> , fragment
19	$m/z$ 966.45	at 1289 s	$C_{44}H_{72}NO_{22}^+$	225.9	3.0	<sup>1</sup> nicotinoside II, [M + NH <sub>4</sub> ] <sup>+</sup> , fragment
20	$m/z$ 468.21	at 677 s	$C_{25}H_{32}N_3O_6^+$	7.8	2.6	<sup>3</sup> unidentified spermidine conjugate, [M + H] <sup>+</sup>

<sup>a</sup> Elemental formulas (El. F.) were calculated using Smart Formula. The absolute mass error (mDa) and the SigmaFit value ( $m\sigma$ ) are reported. Numbers in the compound name column refer to the different annotation levels. iso., isomer.

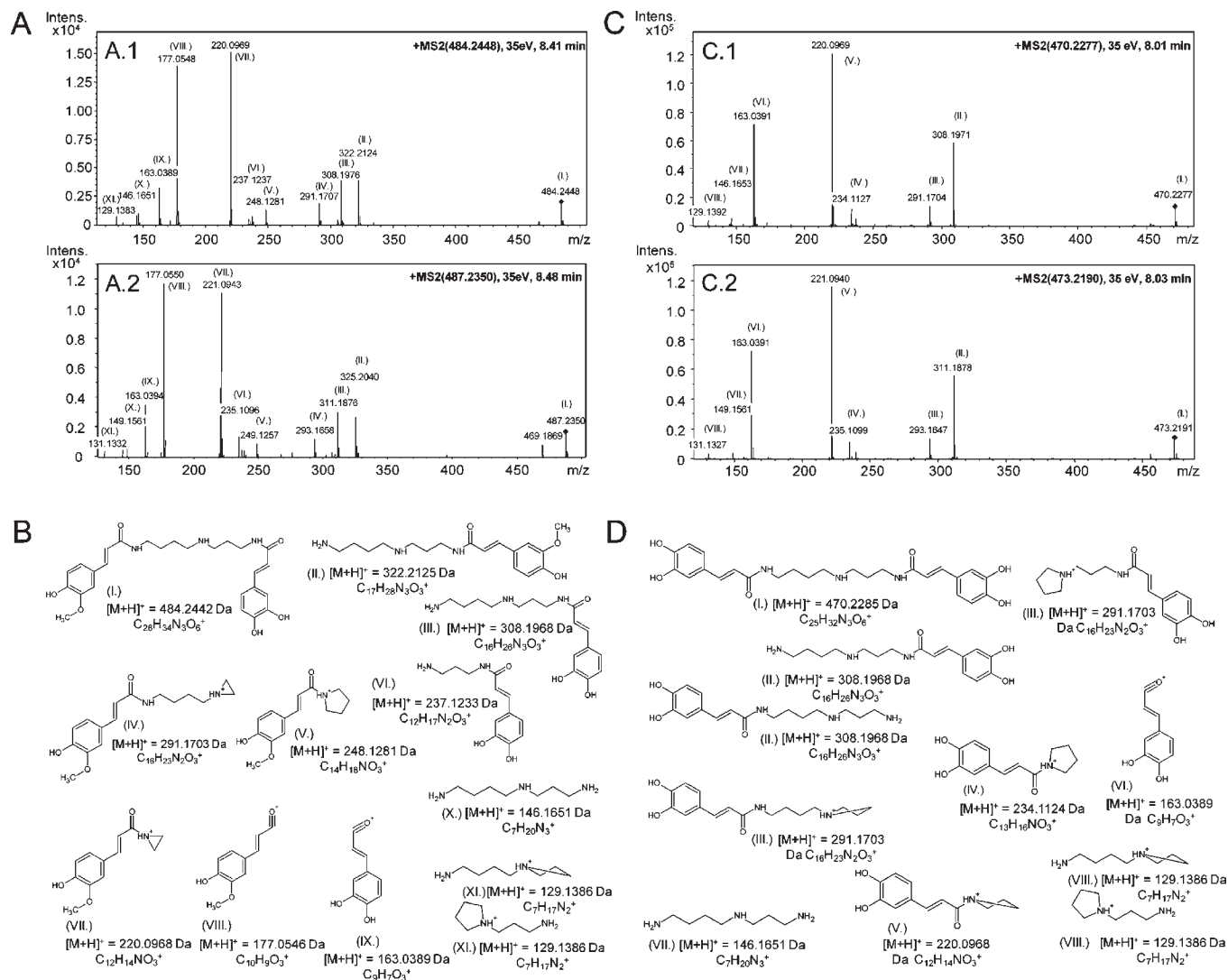


**Figure 4.** MS/MS<sup>+</sup> analysis of two ions increasing in intensity 5 days after simulated herbivory. (A) MS/MS<sup>+</sup> spectra recorded with a collision energy of 35 eV on a maXis qTOF-MS for 484.2448 *m/z* (A.1)/470.2277 *m/z* (C.1) and the corresponding <sup>15</sup>N-labeled parent ion 487.2350 (A.2, 3 nitrogen-containing parent ion)/473.2190 *m/z* (C.2, 3 nitrogen-containing parent ion). (B and D) Putative structures, predicted elemental formulas, and calculated masses (Da) for the parent ion and the major collision-induced ion fragments.

the extraction buffer were chosen to evaluate measurements. Quantifier ions for leaf metabolites were detected and integrated as individual extracted ion chromatogram traces. The electrospray ionization (ESI) source operating in positive ionization mode generated three major adduct types corresponding to the gain of an H<sup>+</sup>, a NH<sub>4</sub><sup>+</sup>, or a Na<sup>+</sup>. The average mass error, calculated after 20-point recalibration of each chromatogram with a sodium formate solution, was 1.5 ± 1.0 mDa for the 22 leaf analytes, 1.13 mDa for atropine, and 0.82 mDa for reserpine. The average maximum *Rt* shift was of 5.9 ± 4.7 s. Atropine and reserpine had a maximum retention time (*Rt*) shift of 0.05 s and of 0.03 s, respectively. The average relative SD (RSD) of the 22 quantifier ion un-normalized intensities was 6.2 ± 4.2%. RSD values calculated from the integration of atropine and reserpine were 9.1% and of 4.9%, respectively. None of the selected metabolites were in the saturation range.

**Mass Signal Bucketing and Principal Component Analysis.** The method was then used to investigate metabolic adjustments in *N. attenuata* leaves during insect attack. To mimic this stress, we used a standardized procedure consisting of wounding leaves with a fabric pattern wheel and applying insect oral secretions (W+OS) (Figure 2). This procedure has already been shown to

recapitulate to a large extent herbivory-specific changes in phyto-hormone, volatile, transcript, and protein levels (5).

Representative chromatograms for each sample class and the data analysis work-flow are presented in Figure 2. We initially used the Profile Analysis software to detect candidate compounds discriminating sample groups, as previously described in Krug et al. (16). The data set was processed from 60 to 1500 s in the mass range *m/z* 90 to 1400 by advanced bucketing. During advanced bucketing, compounds with related isotopes and different charge states as well as chromatographic peak information are the input for the bucket table. Here, this procedure generated 367 consistent buckets (i.e., detected in 4 out of the 5 biological replicates of each sample classes, with a signal-to-noise ratio above 3). Each bucket was subsequently normalized to the total intensity (sum of all bucket values) in an analysis.

Principal component analysis (PCA) was used as an unsupervised method to produce interpretable projections of the samples in a reduced dimensionality (scores plot) and to reveal buckets influencing group separation (loadings plot). To correct for a nonconstant signal variance, the data set was scaled using the PARETO method. The two first principal components (PCs) extracted accounted for ~80% of the total variance existing in the

sample population. As expected, untreated (control 5 days) and W+OS-treated leaf samples collected after 5 days (W+OS 5 days) were the best separated, mainly according to PC1 (Figure 3). In contrast, samples collected after 1 h (control 1 h and W+OS 1 h) were not efficiently separated, and examining other PCs which accounted for a lower amount of variance did not improve their separation on the score plot. These classes were nevertheless segregated on a PCA score plot when analyzing preliminary data recorded using the negative ionization mode (data not shown). Jasmonates which are known to accumulate after wounding or insect attack and are well-ionized in the negative mode may account for the differences existing between the control 1 h and W+OS 1 h samples (8). Future work will examine early metabolic adjustments detected in the negative ionization mode.

**Annotation of W+OS-Elicited Buckets Influencing the PCA Model.** To get a first overview of the metabolites upregulated 5 days after the W+OS treatment, we first considered buckets exhibiting the strongest positive loading values calculated for PC1. Figure 3B, C, and D summarizes the different steps in the examination of these buckets. Buckets assembled around  $m/z$  484.24 at 683 s (characterized as  $N'$ -caffeoyl- $N''$ -feruloyl-spermidine, see below) and  $m/z$  470.23 at 670 s (characterized as a  $N'$ , $N''$ -dicafeoyl-spermidine isomer) are presented as examples. These two buckets increased in intensity 5 days after elicitation by W+OS as visualized from the bucket statistic panels (normalized bucket intensity across samples) and EIC traces. Calculated elemental formulas for these two buckets ( $m/z$  484.24,  $C_{26}H_{34}N_3O_6^+$ ;  $m/z$  470.23,  $C_{25}H_{32}N_3O_6^+$ ) were ranked on the basis of their mass accuracy (2.5 mDa and 1.8 mDa, respectively) and on the fit of their calculated isotope patterns (32.0  $m\sigma$  and 19.1  $m\sigma$ , respectively).

Elemental formulas and putative annotations are provided in Table 1 for the 20 buckets exhibiting the strongest positive loadings on PC1 in the group W+OS/5days. In the case of phenylpropanoid-polyamine conjugates, the number of nitrogen atoms for each of the considered parent ions was confirmed by the HPLC-ESI/TOF-MS analysis of a pooled leaf extract of *N. attenuata* plants grown exclusively on the  $K^{15}NO_3$  substrate (19). In addition to the molecular formula, targeted CID-MS/MS measurements of pseudomolecular ions or in-source fragments add significant information that helps to characterize a compound. CID-MS/MS analyses were performed on a maXis qTOF-MS for most of the parent ions mentioned in Table 1. Figure 4 shows the MS/MS<sup>+</sup> spectra recorded with a collision energy of 35 eV for the two buckets presented in Figure 3 ( $m/z$  484.2448 at 699 s and  $m/z$  470.2333 at 675 s) and for the corresponding parent ions measured after  $^{15}N$ -isotope labeling. On the basis of the interpretation of their accurate mass, on the number of nitrogen atoms, and on the presence of characteristic fragments at  $m/z$  147.0440 ( $C_9H_7O_2^+$ , coumaroyl residue),  $m/z$  163.0389 ( $C_9H_7O_3^+$ , caffeoyl residue), and  $m/z$  177.0546 ( $C_{10}H_9O_3^+$ , feruloyl residue), these two compounds were characterized as  $N'$ , $N''$ -dicafeoyl-spermidine and  $N'$ -caffeoyl- $N''$ -feruloyl-spermidine, respectively (20). Structural rearrangements during CID-MS/MS analyses did not allow the unequivocal assignment of the phenylpropanoid residues to the  $N_1$ ,  $N_5$ , or  $N_{10}$  positions of spermidine (20). Light exposure of a  $N$ -caffeoyl-putrescine standard synthesized according to Matsuda et al. (21) revealed that the second eluting isomer at 262 s, which was not properly extracted by Profile Analysis, resulted from light-dependent isomerization. The pseudomolecular ion corresponding to the compound bucket  $m/z$  347.1965 at 685 s ( $C_{19}H_{27}N_2O_4^+$ ) has a caffeoyl moiety and contains two nitrogens. We hypothesized that this compound corresponds to a metabolite of  $N$ -caffeoyl-putrescine. Nicotine was identified by comparison with a commercial standard. Examination of the MS/MS spectra obtained from the  $^{15}N$ -isotope labeled nicotine did not support the structural

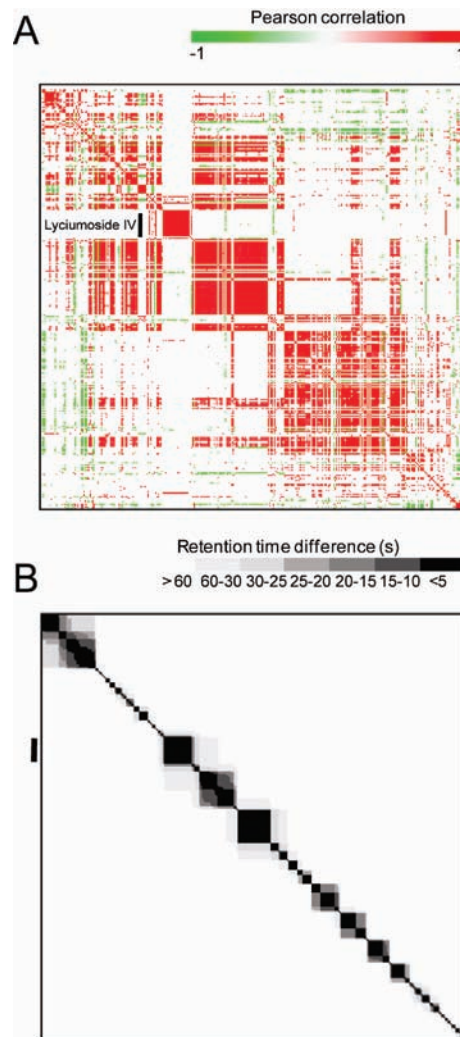


**Figure 5.** Examination of mass signal relationships for annotation. (A) Heat map of the Pearson correlation of mass feature  $\times$  mass feature calculated for 334 mass features detected in 20 samples. (B) Retention time difference matrix.

prediction reported in the literature (22) for the ion fragment at 120.0807  $m/z$ . We propose that this fragment corresponds to  $C_8H_{10}N^+$ .

Diterpene glycosides of *N. attenuata* consist of a acyclic  $C_{20}$  hydroxygeranylinalool backbone conjugated to one or two sugar moieties (glucose and rhamnose) via bonds at the C-3 and C-17 hydroxylated carbons. Diterpene glycosides can furthermore be mono- or dimalonylated (Figure 1B) (23). Interpreted NMR spectra for nicotianosides I and II are reported in this earlier study from our group. The advanced bucketing algorithm is not able to assemble in-source fragments. Diterpene glycosides' intense in-source fragmentation as well as, in some cases, partial coelution can render relatively difficult the unequivocal association of common fragments to a specific diterpene glycoside compound. CID-induced fragmentation measurements of diterpene glycosides were only obtained for the  $[M + Na]^+$  adduct ions.

In general, to test the relationship existing between in-source fragments over the complete data set, we performed a correlation analysis (Figure 5). The rationale is that mass fragments derived from the same parent ion exhibit strict mathematical relationships. Three hundred thirty-four mass features picked using XCMS were used as input variables since in contrast to the buckets generated by Profile Analysis, they consist strictly of a unique  $m/z$  at a unique

**Table 2.** Predicted Cluster of Mathematically and Chromatographically (RT Difference, 5 s) Related Mass Features for Lyciumoside IV<sup>a</sup>

mass	cor. ion	pears. cor.	mass diff.	pred. rel.
271.240	435.309	0.995	164.069	deoxy-hexose, C <sub>6</sub> O <sub>5</sub> H <sub>12</sub>
759.414	597.361	0.976	162.052	hexose, C <sub>6</sub> O <sub>5</sub> H <sub>10</sub>
289.251	451.304	0.988	162.053	hexose, C <sub>6</sub> O <sub>5</sub> H <sub>10</sub>
290.254	272.244	0.946	18.010	H <sub>2</sub> O
418.303	417.299	0.996	1.003	C <sup>13</sup>
435.309	597.361	0.997	162.051	hexose, C <sub>6</sub> O <sub>5</sub> H <sub>10</sub>
215.178	271.240	0.983	56.062	
272.244	418.303	0.991	146.058	deoxy-hexose-H <sub>2</sub> O, C <sub>6</sub> O <sub>4</sub> H <sub>10</sub>
399.289	417.299	0.998	18.010	H <sub>2</sub> O
597.361	579.351	0.995	18.010	H <sub>2</sub> O
309.117	417.299	0.991	108.181	
149.133	451.304	0.926	302.171	
451.304	433.293	0.954	18.0103	H <sub>2</sub> O
433.29	579.351	0.969	146.057	deoxy-hexose-H <sub>2</sub> O, C <sub>6</sub> O <sub>4</sub> H <sub>10</sub>
417.299	399.289	0.998	18.010	H <sub>2</sub> O
579.351	597.361	0.991	18.010	H <sub>2</sub> O
598.365	597.361	0.995	1.003	2C <sup>13</sup>
796.456	794.451	0.996	2.004	2C <sup>13</sup>
794.452	799.407	0.833	4.955	Na/NH <sub>4</sub>
795.455	794.451	0.998	1.003	C <sup>13</sup>
799.407	794.451	0.833	4.955	Na/NH <sub>4</sub>

<sup>a</sup> For each of the mass features composing the Lyciumoside IV cluster, the most correlated (Pearson correlation) mass feature within the cluster is reported as well as the mass difference calculated for each mass pair. According to the mass difference and literature reports, a relationship is predicted. cor. ion, correlated ion; Pears. cor., Pearson correlation; mass diff., mass difference; pred. rel., predicted relationship.

time point. Out of the 111556 possible metabolite pairs, 2551 pairs were significantly correlated ( $P$ -value < 0.05). As expected, clusters of high correlation coefficients were observed for masses at close (< 5 s) or similar  $Rt$ . Mass differences between individual pairs within these clusters were determined and used to predict their likely relationships (lyciumoside IV, **Figure 5** and **Table 2**). In practice, mass differences between pairs of correlated masses of this cluster were searched, using an Excel spreadsheet, versus well described adducts and neutral losses for a predetermined threshold fixed to 0.005 Da. This procedure was routinely carried out in complement with MS/MS measurements.

**Two-Factorial ANOVA and Calculated Fold Changes.** We performed a two-factorial ANOVA (time and treatment) of the bucket table exported from Profile Analysis to calculate the degree of significance of the changes in bucket intensities. One hundred seventy-three buckets were differentially regulated for at least one of the factors or their interaction ( $P$ -value < 0.05). These 173 buckets were sufficient to almost completely discriminate sample classes during hierarchical clustering using the Euclidean distance as a clustering metric (**Figure 6**). The Venn diagram presented in **Figure 6** summarizes the repartitioning of the differentially regulated buckets. One hundred twenty-eight buckets were detected to be differentially regulated when considering the time effect and 85 significantly affected by the W+OS treatment. Differences between control samples are harvested after 1 h and 5 days were assumed to be due to leaf aging, as previously reported notably for diterpene glycosides (23). Buckets with a normalized intensity > 10,000, a retention time in the range of 120–1400 s, and a fold change > 1.5 or < 0.67 ( $P$ -value < 0.05) for at least one of the factors or their interaction are reported in **Table 3**. The nature of these differentially regulated mass signals overlaps in many cases with those detected when independently processing the data set by XCMS and performing the same statistical analysis.

As has been previously reported, W+OS-elicitation significantly induced nicotine production. The intensity of this induction

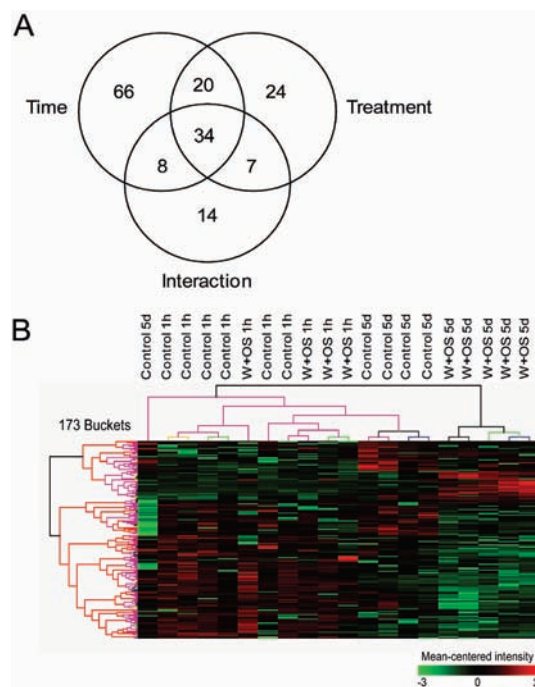


**Figure 6.** Two-factorial ANOVA and hierarchical clustering of the buckets extracted with Profile Analysis. **(A)** Venn diagrams summarizing buckets found statistically regulated during a two-factorial (time and treatment) ANOVA ( $P$ -value < 0.05). **(B)** Hierarchical clustering (complete linkage) after mean-centering using the Euclidean distance as the clustering metric of the 173 buckets statistically regulated. The robustness of the clustering, calculated from 5000 iterations, is depicted by the color of the tree branches (black, 100% support; gray, 90–100%, blue, 80–90%; green, 70–80%; yellow, 50–70%; pink, 0–50%; red, 0%).

was in agreement with the previous results published by our group (2). As previously observed from the PCA loading plot, phenylpropanoid–polyamine conjugates were the most consistently and strongly induced leaf metabolites upon W+OS elicitation. Several transcriptomic studies have previously demonstrated that transcripts encoding enzymes in the phenylpropanoid and polyamine pathways are among those reaching their highest levels during insect feeding (24). Upregulation of the expression of these genes is known to require intact production and perception of jasmonic acid, the central signaling molecule controlling the deployment of antiherbivore defenses in plants (25). Here, *N*-caffeoyl-putrescine was the most strongly upregulated phenylpropanoid–polyamine conjugate upon W+OS treatment. This compound has recently been shown to significantly decrease the performance of lepidopteran larvae when sprayed onto *N. attenuata* plants deficient in phenolic production (4). The mechanisms by which polyamine conjugates may deter insect herbivores remain largely unknown. Interestingly, certain plant phenylpropanoid conjugates of spermidine are structurally similar to those found in the venoms of certain spiders and wasps and have been shown to block glutamate receptors and thereby attenuate synaptic transmission at insect neuromuscular synapses (26). In addition to *N*-caffeoyl-putrescine, the compound at  $m/z$  347.19 at 684.5 s and unidentified spermidine conjugates at  $m/z$  502.25 at 525.4 s and  $m/z$  530.25 at 600.1 s were those for which the largest fold change was calculated. Assigning defensive or homeostatic functions within the phenylpropanoid polyamine conjugate pathway to these metabolites will be the topic of further investigations. Compound buckets  $m/z$  623.31 at 1267 s,  $m/z$  851.40 at 1408 s, and  $m/z$  621.32 at 1439 s decreasing in intensity after the W+OS treatment could not be annotated in the context of this study.

Table 3. Statistical Significance and Fold Change of Major Differentially Regulated Buckets<sup>a</sup>

Bucket	El. F.	Compound	P-value			Fold-change			
						Treatment		Fold-change Time	
			Time	Treat.	Inter.	1h	5d	Control	W+OS
<i>m/z</i> 163.12 at 124 s	C <sub>10</sub> H <sub>13</sub> N <sub>2</sub> <sup>+</sup>	Nicotine, [M+H] <sup>+</sup>	n.s.	2.0E-03	n.s.	1.1	1.2	0.9	1.1
<i>m/z</i> 490.18 at 126 s	C <sub>17</sub> H <sub>32</sub> NO <sub>15</sub> <sup>+</sup>	<sup>4</sup> Unknown, [M+H] <sup>+</sup>	3.3E-08	5.3E-03	n.s.	0.7	0.8	0.4	0.4
<i>m/z</i> 702.26 at 128 s	C <sub>24</sub> H <sub>48</sub> NO <sub>22</sub> <sup>+</sup>	<sup>4</sup> Unknown, fragment	3.5E-02	7.0E-03	1.8E-02	1.0	0.4	1.0	0.4
<i>m/z</i> 251.14 at 192 s	C <sub>13</sub> H <sub>19</sub> N <sub>3</sub> O <sub>3</sub> <sup>+</sup>	<sup>3</sup> N-Caffeoyl-putrescine, [M+H] <sup>+</sup>	7.5E-08	1.6E-07	2.7E-07	1.3	10.1	1.8	14.0
<i>m/z</i> 502.25 at 525 s	C <sub>33</sub> H <sub>52</sub> N <sub>3</sub> O <sub>2</sub> <sup>+</sup>	<sup>4</sup> Unidentified spermidine conjugate, [M+H] <sup>+</sup>	2.4E-10	1.8E-09	6.0E-09	2.1	7.5	4.3	15.0
<i>m/z</i> 350.21 at 535 s	C <sub>18</sub> H <sub>28</sub> N <sub>3</sub> O <sub>4</sub> <sup>+</sup>	<sup>4</sup> Unidentified spermidine conjugate, [M+H] <sup>+</sup>	2.5E-05	4.2E-06	4.3E-05	1.4	4.4	1.1	3.5
<i>m/z</i> 500.24 at 554 s	C <sub>26</sub> H <sub>34</sub> N <sub>3</sub> O <sub>7</sub> <sup>+</sup>	<sup>3</sup> Monohydrated N',N''-di-feruloyl-spermidine, [M+H] <sup>+</sup>	5.7E-05	8.0E-04	1.9E-03	1.5	4.2	3.2	8.7
<i>m/z</i> 530.25 at 600 s	C <sub>27</sub> H <sub>30</sub> N <sub>3</sub> O <sub>8</sub> <sup>+</sup>	<sup>4</sup> Unidentified spermidine conjugate, [M+H] <sup>+</sup>	1.9E-05	2.9E-05	4.2E-05	1.2	7.9	1.3	9.1
<i>m/z</i> 470.23 at 632 s	C <sub>25</sub> H <sub>32</sub> N <sub>3</sub> O <sub>6</sub> <sup>+</sup>	<sup>3</sup> N',N''-Di-caffeoyl-spermidine, [M+H] <sup>+</sup> , isomer#1	9.8E-05	1.6E-04	4.8E-03	1.2	1.9	1.3	2.0
<i>m/z</i> 470.23 at 657 s	C <sub>25</sub> H <sub>32</sub> N <sub>3</sub> O <sub>6</sub> <sup>+</sup>	<sup>3</sup> N',N''-Di-caffeoyl-spermidine, [M+H] <sup>+</sup> , isomer#2	5.1E-06	6.6E-06	1.6E-04	1.3	2.4	1.3	2.4
<i>m/z</i> 470.23 at 675 s	C <sub>25</sub> H <sub>32</sub> N <sub>3</sub> O <sub>6</sub> <sup>+</sup>	<sup>3</sup> N',N''-Di-caffeoyl-spermidine, [M+H] <sup>+</sup> , isomer#3	2.5E-06	3.0E-04	1.9E-04	0.9	2.6	1.7	4.7
<i>m/z</i> 468.21 at 677 s	C <sub>25</sub> H <sub>30</sub> N <sub>3</sub> O <sub>6</sub> <sup>+</sup>	<sup>4</sup> Unidentified spermidine conjugate, [M+H] <sup>+</sup>	2.8E-03	1.6E-04	6.3E-04	1.2	3.8	0.8	2.7
<i>m/z</i> 347.19 at 684 s	C <sub>19</sub> H <sub>27</sub> N <sub>2</sub> O <sub>4</sub> <sup>+</sup>	<sup>4</sup> Unidentified putrescine conjugate, [M+H] <sup>+</sup>	4.6E-03	1.3E-02	1.8E-02	1.3	5.7	2.3	10.0
<i>m/z</i> 731.18 at 688 s	C <sub>32</sub> H <sub>30</sub> O <sub>18</sub> Na <sup>+</sup>	<sup>1</sup> Chlorogenic acid dimer, [M+Na] <sup>+</sup>	2.8E-02	n.s.	n.s.	1.1	0.6	0.7	0.4
<i>m/z</i> 484.24 at 699 s	C <sub>26</sub> H <sub>34</sub> N <sub>3</sub> O <sub>6</sub> <sup>+</sup>	<sup>3</sup> N'-Caffeoyl-N''-feruloyl-spermidine, [M+H] <sup>+</sup>	3.8E-04	1.6E-04	8.5E-04	1.4	5.0	1.2	4.2
<i>m/z</i> 409.18 at 726 s	C <sub>16</sub> H <sub>20</sub> N <sub>2</sub> O <sub>10</sub> <sup>+</sup>	<sup>4</sup> Unknown, [M+H] <sup>+</sup>	1.4E-04	n.s.	4.5E-03	1.2	0.7	2.3	1.2
<i>m/z</i> 498.26 at 727 s	C <sub>27</sub> H <sub>30</sub> N <sub>3</sub> O <sub>6</sub> <sup>+</sup>	<sup>3</sup> N',N''-Di-feruloyl-spermidine, [M+H] <sup>+</sup> , isomer#1	1.4E-06	1.4E-03	1.6E-04	0.9	1.5	1.2	1.8
<i>m/z</i> 498.26 at 747 s	C <sub>27</sub> H <sub>30</sub> N <sub>3</sub> O <sub>6</sub> <sup>+</sup>	<sup>3</sup> N',N''-Di-feruloyl-spermidine, [M+H] <sup>+</sup> , isomer#2	3.1E-07	5.4E-04	4.8E-04	1.0	1.6	1.4	2.2
<i>m/z</i> 611.16 at 834 s	C <sub>27</sub> H <sub>31</sub> O <sub>16</sub> <sup>+</sup>	<sup>1</sup> Rutin, [M+H] <sup>+</sup>	3.3E-09	6.2E-03	9.6E-04	1.0	0.7	0.8	0.5
<i>m/z</i> 471.17 at 1186 s	C <sub>18</sub> H <sub>31</sub> O <sub>14</sub> <sup>+</sup>	<sup>1</sup> Lyciumoside IV, fragment	n.s.	n.s.	4.1E-02	1.5	0.3	2.7	0.6
<i>m/z</i> 1031.5 at 1206 s	C <sub>47</sub> H <sub>70</sub> O <sub>23</sub> Na <sup>+</sup>	<sup>3</sup> Nicotianoside IV, [M+Na] <sup>+</sup>	2.0E-06	8.3E-03	2.8E-02	1.2	1.7	2.9	4.1
<i>m/z</i> 271.24 at 1219 s	C <sub>20</sub> H <sub>31</sub> <sup>+</sup>	<sup>3</sup> Nicotianoside VII, fragment	3.6E-02	n.s.	n.s.	1.3	1.5	1.7	2.0
<i>m/z</i> 625.32 at 1228 s	C <sub>32</sub> H <sub>40</sub> O <sub>12</sub> <sup>+</sup>	<sup>1</sup> Lyciumoside I, fragment	3.1E-04	5.1E-04	n.s.	0.7	0.5	0.7	0.5
<i>m/z</i> 885.40 at 1244 s	C <sub>41</sub> H <sub>60</sub> O <sub>19</sub> Na <sup>+</sup>	<sup>3</sup> Nicotianoside I, [M+Na] <sup>+</sup>	2.2E-02	n.s.	n.s.	0.7	0.9	1.7	2.1
<i>m/z</i> 623.31 at 1267 s	C <sub>32</sub> H <sub>47</sub> O <sub>12</sub> <sup>+</sup>	<sup>4</sup> Unknown	n.s.	2.0E-02	n.s.	0.6	0.7	0.9	0.9
<i>m/z</i> 931.41 at 1289 s	C <sub>44</sub> H <sub>67</sub> O <sub>21</sub> <sup>+</sup>	<sup>1</sup> Nicotianoside II, fragment	n.s.	1.3E-02	n.s.	1.8	3.1	1.1	1.9
<i>m/z</i> 603.26 at 1316 s	C <sub>26</sub> H <sub>44</sub> O <sub>14</sub> Na <sup>+</sup>	<sup>3</sup> Sucrose ester#1, [M+Na] <sup>+</sup>	1.5E-03	3.7E-04	2.0E-03	1.0	0.6	1.0	0.6
<i>m/z</i> 709.34 at 1381 s	C <sub>43</sub> H <sub>69</sub> O <sub>9</sub> <sup>+</sup>	<sup>4</sup> Unknown	4.1E-02	2.1E-02	n.s.	0.5	0.8	1.2	2.1
<i>m/z</i> 851.40 at 1408 s	C <sub>50</sub> H <sub>59</sub> O <sub>12</sub> <sup>+</sup>	<sup>4</sup> Unknown	n.s.	3.0E-06	7.1E-03	0.7	0.5	1.2	0.8
<i>m/z</i> 621.32 at 1439 s	C <sub>33</sub> H <sub>49</sub> O <sub>11</sub> <sup>+</sup>	<sup>4</sup> Unknown	4.3E-02	1.0E-05	n.s.	0.7	0.4	1.0	0.6
<i>m/z</i> 645.27 at 1449 s	C <sub>29</sub> H <sub>50</sub> O <sub>14</sub> Na <sup>+</sup>	<sup>3</sup> Sucrose ester#4, [M+Na] <sup>+</sup>	n.s.	2.0E-02	n.s.	0.8	0.6	1.2	0.8
<i>m/z</i> 631.29 at 1468 s	C <sub>28</sub> H <sub>48</sub> O <sub>14</sub> Na <sup>+</sup>	<sup>3</sup> Sucrose ester#3, [M+Na] <sup>+</sup>	n.s.	1.8E-02	3.0E-03	1.0	0.7	1.1	0.7

<sup>a</sup> Buckets with a normalized intensity >10,000, a retention time in the range of 120–1400 s, and a fold-change >1.5 or <0.67 (two-factorial ANOVA *P*-value <0.05, time and treatment as factors and their interaction) for at least one of the factors or their interaction are reported. Nicotine, a typical defense marker from *Nicotiana attenuata* was reported, although the calculated fold-changes for this metabolite were below 1.5. The shading of cells is proportional to the fold change values. Numbers in the compound name column refer to the different annotation levels. El. F., elemental formulas; Inter., interaction; n.s., non significant.



In *N. attenuata*, total diterpene glycoside concentrations in leaves increase after treatment with the plant stress hormone methyl jasmonate or feeding by *M. sexta* larvae (23, 27). These metabolites, which occur in the range of a few milligrams per gram fresh weight of young rosette leaves, strongly alter insect performance in laboratory and field conditions (3, 23). Here, levels of nicotianosides I and IV, two monomalonylated diterpene glycosides, and nicotianoside II and VII, two dimalonylated diterpene glycosides, increased in leaf tissues over the 5 days of the experiment. Concentrations of three of them, namely, nicotianosides II, IV, and VII, were significantly more elevated after the leaves had been treated by W+OS. Thus, the W+OS treatment resulted for nicotianosides II, IV and VII in 1.8-, 1.3 and 1.2-fold increases, respectively, after 1 h and 3.1-, 1.7- and 1.5-fold increases, respectively, after 5 days compared to those in controls. As previously reported and in agreement with malonylation being a W+OS-inducible step in diterpene glycoside metabolism, the amounts of nonmalonylated diterpene glycosides, such as lyciumoside IV, significantly decreased after treatment. Levels of lyciumoside IV, while being 1.5-fold increased in W+OS treated leaves compared to those in controls after 1 h, represented only 30% of those in controls after 5 days. Translocation of certain diterpene glycoside compounds has also been evoked to interpret the qualitative and quantitative changes in the local diterpene glycoside panel after W+OS elicitation. The present study certainly minimizes the possibility of diterpene glycoside translocation as five leaves per plants were treated and subsequently pooled before analysis. This particularity of the experimental design might explain small quantitative differences in the amplitude of the changes in diterpene glycoside concentrations observed in the present study compared to what we have previously reported (3, 23).

The pool of sucrose esters decreased after the leaves had been treated by W+OS. Sucrose esters are metabolites exuded by the glandular trichomes of many species in Solanaceae and which can represent up to 15% of the leaf dry mass in *Nicotiana* species (28). The decreases in sucrose ester levels may be explained by the repression of sucrose ester biosynthesis rather than by the removal of these surface chemicals by the pattern wheel treatment as the differences with control levels were more pronounced after 5 days than after 1 h. Acyl moieties of sucrose esters are constituted by branched short chain fatty acids ranging from C<sub>3</sub> to C<sub>6</sub> (Figure 1A). These fatty acids originate from branched-chain acyl-CoAs produced from keto-acids during photosynthetic carbon dioxide assimilation. We speculate that the decrease of the sucrose ester pool is linked to the reduction of the photosynthetic activity occurring in herbivore-damaged leaves (29). It is moreover conceivable that the local decrease of the photosynthetic flux was amplified by the fact that 5 leaves per plants were treated. Carbon reallocation to roots in response to leaf damage has been shown to occur in several plant species. This physiological process which has been shown to facilitate tolerance to insect herbivory in *N. attenuata* (30) might also influence the exudation of sucrose esters onto the leaf surface. Sucrose esters exhibited negative loading values on PC1 and were not listed within the initial ion buckets presented in Table 1.

In addition to identifying abundant phytochemicals, our work reveals subtle significant changes occurring in the concentrations of metabolites that occur at much lower levels. Even though these low-abundance metabolites could not be fully analyzed in the context of this study, the interpretation of negative ionization data spectra and the refinement of the time-sampling will help in this process. Future work will aim, using the tools and calculations presented here, at exploring more deeply the reconfigurations of the plant's metabolome and how they influence its resistance to herbivores.

## ACKNOWLEDGMENT

We thank E. Rothe and B. Berger for helping with the plant treatment and sample extraction, B. Berger and S. Mitra for suggestions on an earlier version of the manuscript, and A. Weinhold for sharing his knowledge on sucrose ester analysis.

**Supporting Information Available:** Linearity of the detector response for 12 highly abundant metabolites; PCA projection plots for the three first principal components; MS/MS<sup>+</sup> analysis of parent ions characterized as *N',N''*-diferuloyl-spermidine and *N''*-coumaroyl-*N''*-caffeoyl-spermidine; MS/MS<sup>+</sup> spectra of herbivory-regulated compounds. Bucket table exported from Profile Analysis; XCMS mass feature table and statistical analysis; Pearson correlation and retention difference matrices; and two-factorial ANOVA results. This material is available free of charge via the Internet at <http://pubs.acs.org>

## LITERATURE CITED

- (1) Karban, R.; Baldwin, I. T. *Induced Responses to Herbivory*; The University of Chicago Press: Chicago, IL, 1997.
- (2) Steppuhn, A.; Gase, K.; Krock, B.; Halitschke, R.; Baldwin, I. T. Nicotine's defensive function in nature. *PLoS Biol.* **2004**, *2* (8), E217.
- (3) Jassbi, A. R.; Gase, K.; Hettenhausen, C.; Schmidt, A.; Baldwin, I. T. Silencing geranylgeranyl diphosphate synthase in *Nicotiana attenuata* dramatically impairs resistance to tobacco hornworm. *Plant Physiol.* **2008**, *146* (3), 974–986.
- (4) Kaur, H.; Heinzel, N.; Schottner, M.; Baldwin, I. T.; Galis, I. R2R3-NaMYB8 regulates the accumulation of phenylpropanoid-polyamine conjugates, which are essential for local and systemic defense against insect herbivores in *Nicotiana attenuata*. *Plant Physiol.* **2010**, *152* (3), 1731–1747.
- (5) Halitschke, R.; Gase, K.; Hui, D.; Schmidt, D. D.; Baldwin, I. T. Molecular interactions between the specialist herbivore *Manduca sexta* (Lepidoptera, sphingidae) and its natural host *Nicotiana attenuata*. VI. Microarray analysis reveals that most herbivore-specific transcriptional changes are mediated by fatty acid-amino acid conjugates. *Plant Physiol.* **2003**, *131* (4), 1894–1902.
- (6) Giri, A. P.; Wunsche, H.; Mitra, S.; Zavala, J. A.; Muck, A.; Svatos, A.; Baldwin, I. T. Molecular interactions between the specialist herbivore *Manduca sexta* (Lepidoptera, Sphingidae) and its natural host *Nicotiana attenuata*. VII. Changes in the plant's proteome. *Plant Physiol.* **2006**, *142* (4), 1621–1641.
- (7) Gaquerel, E.; Weinhold, A.; Baldwin, I. T. Molecular interactions between the specialist herbivore *Manduca sexta* (Lepidoptera, Sphingidae) and its natural host *Nicotiana attenuata*. VIII. An unbiased GCxGC-ToFMS analysis of the plant's elicited volatile emissions. *Plant Physiol.* **2009**, *149* (3), 1408–1423.
- (8) Glauser, G.; Grata, E.; Rudaz, S.; Wolfender, J. L. High-resolution profiling of oxylipin-containing galactolipids in *Arabidopsis* extracts by ultra-performance liquid chromatography/time-of-flight mass spectrometry. *Rapid Commun. Mass Spectrom.* **2008**, *22* (20), 3154–3160.
- (9) Grata, E.; Boccard, J.; Guillaume, D.; Glauser, G.; Carrupt, P. A.; Farmer, E. E.; Wolfender, J. L.; Rudaz, S. UPLC-TOF-MS for plant metabolomics: A sequential approach for wound marker analysis in *Arabidopsis thaliana*. *J. Chromatogr., B* **2008**, *871* (2), 261–270.
- (10) Kaefer, A.; Lingner, T.; Feussner, K.; Gobel, C.; Feussner, I.; Meinicke, P. MarVis: a tool for clustering and visualization of metabolic biomarkers. *BMC Bioinf.* **2009**, *10*, 92.
- (11) Allwood, J. W.; Ellis, D. I.; Heald, J. K.; Goodacre, R.; Mur, L. A. Metabolomic approaches reveal that phosphatidic and phosphatidyl glycerol phospholipids are major discriminatory non-polar metabolites in responses by *Brachypodium distachyon* to challenge by *Magnaporthe grisea*. *Plant J.* **2006**, *46* (3), 351–368.
- (12) Jansen, J. J.; Allwood, J. W.; Marsden-Edwards, E.; van der Putten, W. H.; Goodacre, R.; van Dam, N. M. Metabolomic analysis of the interaction between plants and herbivores. *Metabolomics* **2009**, *5* (1), 150–161.
- (13) Kuzina, V.; Ekstrom, C. T.; Andersen, S. B.; Nielsen, J. K.; Olsen, C. E.; Bak, S. Identification of defense compounds in

- Barbarea vulgaris* against the herbivore *Phyllotreta nemorum* by an ecometabolomic approach. *Plant Physiol.* **2009**, *151* (4), 1977–1990.
- (14) Tautenhahn, R.; Bottcher, C.; Neumann, S. Highly sensitive feature detection for high resolution LC/MS. *BMC Bioinf.* **2008**, *9*, 504.
- (15) Krugel, T.; Lim, M.; Gase, K.; Halitschke, R.; Baldwin, I. T. Agrobacterium-mediated transformation of *Nicotiana attenuata*, a model ecological expression system. *Chemoecology* **2002**, *12* (4), 177–183.
- (16) Krug, D.; Zurek, G.; Schneider, B.; Garcia, R.; Muller, R. Efficient mining of myxobacterial metabolite profiles enabled by liquid chromatography-electrospray ionisation-time-of-flight mass spectrometry and compound-based principal component analysis. *Anal. Chim. Acta* **2008**, *624* (1), 97–106.
- (17) Sumner, L. W.; Amberg, A.; Barrett, D.; Beale, M. H.; Beger, R.; Daykin, C. A.; Fan, T. W. M.; Fiehn, O.; Goodacre, R.; Griffin, J. L.; Hankemeier, T.; Hardy, N.; Harnly, J.; Higashi, R.; Kopka, J.; Lane, A. N.; Lindon, J. C.; Marriott, P.; Nicholls, A. W.; Reily, M. D.; Thaden, J. J.; Viant, M. R. Proposed minimum reporting standards for chemical analysis. *Metabolomics* **2007**, *3* (3), 211–221.
- (18) van den Berg, R. A.; Hoefsloot, H. C.; Westerhuis, J. A.; Smilde, A. K.; van der Werf, M. J. Centering, scaling, and transformations: improving the biological information content of metabolomics data. *BMC Genomics* **2006**, *7*, 142.
- (19) Baldwin, I. T.; Gorham, D.; Schmelz, E. A.; Lewandowski, C. A.; Lynds, G. Y. Allocation of nitrogen to an inducible defense and seed production in *Nicotiana attenuata*. *Oecologia* **1998**, *115* (4), 541–552.
- (20) Youhnovski, N.; Bigler, L.; Werner, C.; Hesse, M. On-line coupling of high-performance liquid chromatography to atmospheric pressure chemical ionization mass spectrometry (HPLC/APCI-MS and MS/MS). The pollen analysis of *Hippeastrum x hortorum* (Amaryllidaceae). *Helv. Chim. Acta* **1998**, *81* (9), 1654–1671.
- (21) Matsuda, F.; Morino, K.; Ano, R.; Kuzawa, M.; Wakasa, K.; Miyagawa, H. Metabolic flux analysis of the phenylpropanoid pathway in elicitor-treated potato tuber tissue. *Plant Cell Physiol.* **2005**, *46* (3), 454–466.
- (22) Pellegrini, M.; Marchei, E.; Rossi, S.; Vagnarelli, F.; Durgbansh, A.; Garcia-Algar, S.; Vall, O.; Pichini, S. Liquid chromatography/electrospray ionization tandem mass spectrometry assay for determination of nicotine and metabolites, caffeine and arecoline in breast milk. *Rapid Commun. Mass Spectrom.* **2007**, *21* (16), 2693–2703.
- (23) Heiling, S.; Schuman, M. C.; Schoettner, M.; Mukerjee, P.; Berger, B.; Schneider, B.; Jassbi, A. R.; Baldwin, I. T. Jasmonate and ppHsystemin regulate key malonylation steps in the biosynthesis of 17-hydroxygeranylinalool diterpene glycosides, an abundant and effective direct defense against herbivores in *Nicotiana attenuata*. *Plant Cell* **2010**, *22* (1), 273–292.
- (24) Schmidt, D. D.; Voelckel, C.; Hartl, M.; Schmidt, S.; Baldwin, I. T. Specificity in ecological interactions: attack from the same lepidopteran herbivore results in species-specific transcriptional responses in two solanaceous host plants. *Plant Physiol.* **2005**, *138* (3), 1763–1773.
- (25) Paschold, A.; Halitschke, R.; Baldwin, I. T. Co(i)-ordinating defenses: NaCOII mediates herbivore-induced resistance in *Nicotiana attenuata* and reveals the role of herbivore movement in avoiding defenses. *Plant J.* **2007**, *51* (1), 79–91.
- (26) Klose, M. K.; Atkinson, J. K.; Mercier, A. J. Effects of a hydroxycinnamoyl conjugate of spermidine on arthropod neuromuscular junctions. *J. Comp. Physiol. A* **2002**, *187* (12), 945–952.
- (27) Keinanen, M.; Oldham, N. J.; Baldwin, I. T. Rapid HPLC screening of jasmonate-induced increases in tobacco alkaloids, phenolics, and diterpene glycosides in *Nicotiana attenuata*. *J. Agric. Food Chem.* **2001**, *49* (8), 3553–8.
- (28) Slocombe, S. P.; Schauvinhold, I.; McQuinn, R. P.; Besser, K.; Welsby, N. A.; Harper, A.; Aziz, N.; Li, Y.; Larson, T. R.; Giovannoni, J.; Dixon, R. A.; Broun, P. Transcriptomic and reverse genetic analyses of branched-chain fatty acid and acyl sugar production in *Solanum pennellii* and *Nicotiana benthamiana*. *Plant Physiol.* **2008**, *148* (4), 1830–46.
- (29) Hermsmeier, D.; Schittko, U.; Baldwin, I. T. Molecular interactions between the specialist herbivore *Manduca sexta* (Lepidoptera, Sphingidae) and its natural host *Nicotiana attenuata*. I. Large-scale changes in the accumulation of growth- and defense-related plant mRNAs. *Plant Physiol.* **2001**, *125* (2), 683–700.
- (30) Schwachtje, J.; Minchin, P. E. H.; Jahnke, S.; van Dongen, J. T.; Schittko, U.; Baldwin, I. T. SNF1-related kinases allow plants to tolerate herbivory by allocating carbon to roots. *Proc. Natl. Acad. Sci. U.S.A.* **2006**, *103* (34), 12935–12940.

---

Received for review May 8, 2010. Revised manuscript received July 20, 2010. Accepted July 21, 2010. This research was supported by the Max Planck Society.